European Polymer Journal 254 (2026) 114780

Contents lists available at ScienceDirect

European Polymer Journal

journal homepage: www.elsevier.com/locate/europolj

Design of polymeric nanoantibiotics: N-acetylcysteine-functionalized PLA-PEG nanoparticles for linezolid and pentamidine delivery

Antonia Nostro [a], Giovanna Ginestra [a], Federica Grasso [a], Massimiliano Cordaro [a], Anna Piperno [a], Angelo Nicosia [b], Angela Scala [a,*]

[a] Department of Chemical, Biological, Pharmaceutical and Environmental Sciences, University of Messina, V.le F. Stagno d'Alcontres 31, 98166 Messina, Italy
[b] Department of Chemical Sciences, University of Catania, Viale A. Doria, 95125 Catania, Italy

ARTICLE INFO

Keywords:
Polyesters
PLA-PEG
CuAAC
Nanoparticles
Drug delivery
MRSA

ABSTRACT

Polymeric nanoparticles bearing multifunctional features, including surface functionalization, hold great promise to address current limitations in antimicrobial drug delivery. Among bioactive ligands, N-acetylcysteine (NAC) and its derivatives have been investigated for their ability to interfere with biofilm formation and to disrupt mature biofilms. Here we propose novel N-acetylcysteine-decorated Nanoantibiotics based on poly(lactic acid)-poly(ethylene glycol) nanoparticles (PLA-PEG-NAC NPs) incorporating Linezolid (LNZ) and Pentamidine (Pent). NAC was selected to target methicillin-resistant *Staphylococcus aureus* (MRSA) biofilm and Pent for broadening the antimicrobial spectrum of LNZ. The PLA-PEG-NAC copolymer was synthesized through a multi-step pathway involving carbonyldiimidazole-mediated amidation, Steglich esterification, and copper(I)-catalyzed azide-alkyne cycloaddition (CuAAC). Successful NAC grafting was confirmed by thiol-ene Michael addition using a crotonyl-substituted BODIPY dye. Nanoparticle's formulation by dialysis achieved encapsulation efficiencies of 12% for LNZ and 20% for Pent, with sustained drug release profiles (78% and 25% cumulative release within 24 h, respectively). Despite the moderate encapsulation efficiency, the observed biological effects closely reflected the drug release profile and the achieved drug loading proved suitable for the aims of the present work. Cytotoxicity assays in Vero cells demonstrated no notable toxicity of PLA-PEG-NAC NPs, either in their drug-loaded or unloaded forms. Encapsulated LNZ preserved its antimicrobial activity, displaying Minimal Inhibitory and Bactericidal Concentrations (MIC and MBC) of 2 μg/mL and 16 μg/mL, respectively, against *S. aureus,* MRSA, *S. epidermidis* and *Enterococcus faecium*. Notably, sub-MIC concentrations of PLA-PEG-NAC@LNZ NPs reduced MRSA biofilm formation more effectively than free LNZ as demonstrated by biomass inhibition (62% *vs* 39%) and fluorescence microscopy. At 8 × MIC, PLA-PEG-NAC@LNZ NPs demonstrated activity against preformed MRSA biofilm either in the early (49% biofilm reduction) and late stages (30–41% biofilm reduction, depending on exposure time). Furthermore, the combined use of PLA-PEG-NAC@LNZ NPs and PLA-PEG-NAC@Pent NPs produced an additive antibacterial effect against *Escherichia coli* supporting the potential of Pent to sensitize Gram-negative bacteria to Gram-positive-targeting antibiotics such as LNZ.

1. Introduction

Functional polymers emerged as key materials in modern nanomedicine due to the presence of one or more specific chemical groups that enable tailored properties, features, and applications [1]. These materials are typically synthesized by the reaction of polymers with biologically active ligands or moieties that confer responsiveness to biological systems.

Although the synthesis of functional polymers with controlled architecture, composition, and molecular weight remains challenging (due to relative complexity and cost) and requires fine control over the polymer-chemistry toolbox [2], a major boost to this research comes from the ability of functional polymers to self-assemble, enabling the formation of supramolecular structures and multifunctional nanoparticles endowed with specific recognition chemical moieties.

Among the various functionalization strategies, the decoration of

* Corresponding author at: Department of Chemical, Biological, Pharmaceutical and Environmental Sciences, University of Messina, V.le F. Stagno d'Alcontres 31, 98166 Messina, Italy.
E-mail address: ascala@unime.it (A. Scala).

https://doi.org/10.1016/j.eurpolymj.2026.114780
Received 24 January 2026; Received in revised form 3 April 2026; Accepted 28 April 2026
Available online 2 May 2026

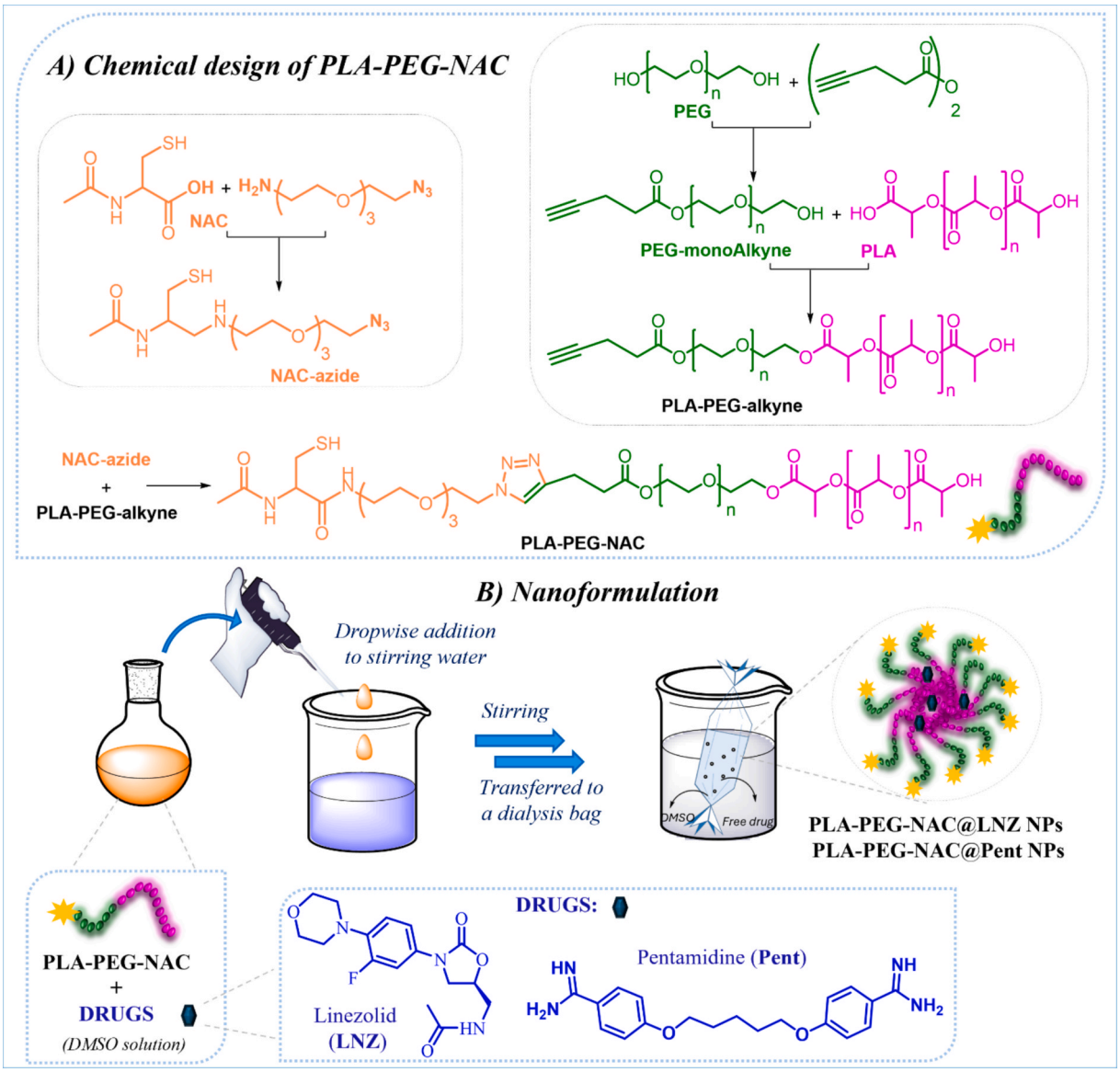

Fig. 1. (A) Synthetic design of PLA-PEG-NAC. (B) Sketched view of Nanoantibiotics formulation. In the inset, the chemical structure of investigated drugs (LNZ and Pent) is also reported.

polymers with cysteine and its derivatives, including N-acetylcysteine or esters, has gained increasing attention since the thiol group plays a crucial role in enhancing the adhesion of polymers to biological tissue, that is critical for materials' functionality, promoting both covalent and non-covalent interactions (*i.e.,* disulfide bonds with other thiol-containing molecules and hydrogen bonds) [3]. Additionally, polymer-cysteine conjugates typically undergo swelling into body fluids promoting material spreading and increasing the availability of thiol groups for disulfide bonding. This behaviour ultimately enhances muco- and tissue-adhesive properties which are particularly advantageous in drug delivery and tissue engineering applications where prolonged residence time and stable anchoring are required.

N-acetylcysteine (NAC) is a thiol-containing mucolytic agent commonly used for the treatment of respiratory infections with antimicrobial properties against both Gram-positive and Gram-negative bacteria (including clinically relevant methicillin-resistant *Staphylococcus aureus,* MRSA) and effectiveness in both disrupting mature biofilms as well as inhibiting biofilm formation (reduction of bacteria adhesion and extracellular matrix production) [4,5].

Biofilms are recognized as a major contributor to chronic and persistent infections as they endow bacteria with resistance to host immune responses and conventional antimicrobial therapies, being usually more virulent than their planktonic counterparts.

The ability of NAC to act as a co-adjuvant in the treatment of bacterial infections points out the importance of achieving a high long-lasting local NAC concentration to maximize the antimicrobial efficacy [6].

However, systemic administration typically results in NAC plasma levels that are markedly lower (around 0.035 mg/mL) than the effective concentrations observed in most antimicrobial studies (between 4 and 80 mg/mL) pointing out the need for alternative strategies for delivering high local concentrations [6]. In this regard, nanotechnology offers promising tools for the controlled and localized delivery of antimicrobials and anti-biofilm agents with the potential to overcome biofilm-associated resistance [7,8]. In fact, engineered nanoparticles encapsulating antibiotics ("Nanoantibiotics") and functionalized with targeting ligands such as NAC exhibit a superior ability compared to conventional antibiotics to penetrate the extracellular matrix, to improve permeability and to deliver antimicrobial agents directly to biofilm-embedded bacteria. Moreover, NAC also exerts a beneficial modulatory effect when

used in combination with some conventional antibiotics [9].

From a synthetic standpoint, several covalent strategies have been described in recent years to synthesize cysteine-polymer conjugates [3] including *grafting to, grafting from, and grafting through* approaches: aminoacids can be conjugated to the polymer following its synthesis (*grafting to)* or they can directly participate in the polymerization as the initiator (*grafting from)* or macromonomer (*grafting through)*.

Among these, the *grafting to* approach is the most commonly used strategy for conjugating cysteine and its derivatives to polymers, exploiting the thiol, amine, or carboxylic groups through thiol-ene, amidation, imidation, and thio-Michael addition reactions. A broad range of polymeric platforms, including hyaluronic acid, chitosan, alginate, polycaprolactone, polyurethane, poly(acrylic acid), poly (ethylene glycol), has been successfully thiolated for biological purposes [3]. These materials, often referred to as thiomers [10], exhibit distinctive mucoadhesive features as a result of intra- and interchain disulfide bond formation within the polymer network and the cysteine residues of mucosal glycoproteins. Such polymer-mucus interactions prolong the residence time of drug delivery systems on mucosal surfaces, thereby enhancing drug absorption and therapeutic effectiveness.

Our recent work investigated the ability of bare PLA-PEG NPs to provide efficient and prolonged delivery of LNZ [11], a synthetic oxazolidinone antibiotic active against Gram-positive bacteria currently employed for the treatment of surgical or multidrug-resistant pulmonary infections caused by vancomycin-resistant *Enterococcus faecium* (VREfm), MRSA, penicillin-resistant pneumococci, and also for treating MDR-*Mycobacterium tuberculosis* infections [12]. Interestingly, our PLA-PEG NPs acted as "LNZ activity enhancer" endowed with inhibitory activity on both planktonic growth and preformed biofilm of MRSA [11]. These biological findings prompted us to design a tailored synthetic strategy for a novel PLA-PEG copolymer featuring suitable end-groups for the covalent attachment of NAC, with the aim of improving antibiofilm performance and permeation.

Moreover, recent literature reported that Pentamidine (Pent), a FDA-approved antiparasitic drug with documented antimicrobial, anti-inflammatory, and anti-cancer activity [13,14], strongly synergized with LNZ against Gram-negative bacteria (*Escherichia coli, Klebsiella pneumoniae, Enterobacter cloacae, Acinetobacter baumannii*) acting as a membrane-targeting sensitizer by disordering (but not completely disrupting) the lipopolysaccharide outer layer and, additionally, inactivating the antibiotic efflux pump [15,16]. However, the clinical use of Pent-based combinations has been limited, so far, by the high doses required and associated toxicity concerns. Nevertheless, recent literature pointed out that specific Pent-LNZ combinations (8–128, 16–64, 32–64, 64–32, 128–32 mg/L) did not exhibit toxicity in mammalian cell models (mouse RAW264.7) and caused less than 3% red blood cell haemolysis at concentrations up to 512 mg/L. Additionally, Pent and LNZ, whether used alone or in combination at 32–512 mg/L, showed no toxicity in the *Galleria mellonella* larvae *in vivo* model, supporting their potential safety and therapeutic relevance [16].

With this in mind, the present study aims to investigate novel Nanoantibiotics, unprecedented in literature, based on a newly synthesized amphiphilic poly(lactic acid)-poly(ethylene glycol)-N-acetylcysteine conjugate (PLA-PEG-NAC, Fig. 1A) able to self-assemble into nanoparticles incorporating LNZ and Pent (PLA-PEG-NAC@LNZ NPs and PLA-PEG-NAC@Pent NPs, respectively, Fig. 1B).

The amphiphilic PLA-PEG copolymer was synthesized by a proper combination of copper-catalyzed azide-alkyne cycloaddition (CuAAC), amide coupling, and Steglich esterification reactions. NAC was covalently linked to the end-groups of PEG to be eventually exposed on the nanocarrier surface. Therefore, the novel cysteine-copolymer conjugate self-assembled in water and its nanoformulation guaranteed −SH group exposure on the nanoparticle surface and the consequent steady adhesion of the nanomaterial to the mucus layer, forming covalent S-S bonds with the mucus cysteine. NAC was selected for destroying MRSA biofilm and, also, for preventing its formation. Moreover, the incorporation of suitable drugs (*i.e.,* LNZ and Pent) was achieved during nanoformulation, leading to PLA-PEG-NAC@LNZ and PLA-PEG-NAC@Pent Nanoantibiotics, respectively. Pent was used for broadening the antimicrobial spectrum of LNZ since it promoted the entry of LNZ (increasing the outer membrane permeability) and its intracellular accumulation (due to the simultaneous inhibition of the efflux pump) in Gram-negative bacteria.

The physicochemical characterization of the newly synthesized PLA-PEG-NAC copolymer and its molecular sub-units was carried out by different techniques including NMR, FT-IR, mass spectrometry, and GPC analyses. The Nanoantibiotics were fully characterized in terms of hydrodynamic diameter, zeta potential, drug loading, encapsulation efficiency, and drug release. The biological profile of PLA-PEG-NAC@LNZ NPs was investigated focusing on: *a)* the evaluation of MIC and MBC against *S. aureus*, MRSA, *S. epidermidis* and *E. faecium* (VRE-fm) strains, *b)* the effect on biofilm formation and on preformed MRSA biofilms at early (8 h) and late (24 h) stages, and *c)* the efficacy in combination with PLA-PEG-NAC@Pent NPs against *E. coli*.

2. Materials and methods

2.1. General

N-acetylcysteine (NAC), 11-azido-3,6,9-trioxaundecan-1-amine, poly(D,L-lactide) (PLA, 10.000–17.000 Da), polyethylene glycol (PEG 2.000 Da), crotonyl chloride, solvents and other reagents were purchased from Merck (Italy).

^{1}H NMR spectra were recorded on a Varian 500 MHz spectrometer at 25°C. FT-IR spectra were registered on a Spectrum Two Perkin Elmer spectrometer equipped with a Universal Attenuated Total Reflectance Accessory (UATR). DLS measurements (size and ζ-potential) were performed on a Malvern Zetasizer prored zsu 3205. Gel permeation chromatography (GPC) experiments were performed using a PL-GPC 110 (Polymer Laboratories), equipped with two Mixed-D and one Mixed-E PL-gel 5 μm columns joined in series. As detectors, a differential refractometer connected in parallel with a UV–Vis spectrophotometer (Hewlett Packard series 1050) were used. The analysis was carried out at 35 ± 0.1°C using THF as eluent (flow rate 1 mL/min). Data acquisition was performed with ASTRA software (version 6.0.1.10, Wyatt Technology). Positive ESI mass spectra were acquired on an API 2000 mass spectrometer (AB-Sciex, Milano, Italy) equipped with an API ion source. The DMSO solutions of the investigated samples were introduced into the source at a flow rate of 5 μL/min. The mass spectra were elaborated with the Analyst software (from AB-Sciex).

2.2. Synthetic procedures

The reactions reported in this study were performed on a 0.5–0.8 g scale; however, the synthetic protocol is expected to be readily scalable due to the use of cost-effective and commercially available reagents.

2.2.1. Synthesis of NAC-azide (3)

NAC (**1**) (500 mg, 3.06 mmol) and CDI (497 mg, 3.06 mmol, 1 equiv) were dissolved in 20 mL THF in a two-neck round-bottom flask under inert atmosphere. The reaction mixture was heated to 75°C and refluxed for 2 h, followed by the addition of 11-azido-3,6,9-trioxaundecan-1-amine (**2**) (668 mg, 3.06 mmol, 1 equiv). The reaction was heated at reflux for 24 h under constant stirring. After cooling to room temperature, the mixture was filtered to recover NAC-azide (**3**) as a brownish solid (764 mg, 70%). ^{1}H NMR (500 MHz, CD_3OD): δ 4.55–4.52 (m, 1H, CH), 3.90–3.84 (m, 2H, CH_2O), 3.73–3.61 (m, 4H, CH_2O), 3.38–3.35 (m, 2H, CH_2N_3), 3.32–3.30 (m, 1H, CH_2SH), 3.15–3.11 (m, 2H, CH_2NH), 3.03–3.00 (m, 1H, CH_2SH), 1.99 (s, 3H, CH_3). ^{13}C NMR (125 MHz, CD_3OD) δ 175.59, 171.57, 70.11, 70.00, 69.80, 66.69, 60.72, 60.16, 54.13, 50.40, 41.52, 39.16, 21.70. ESI-MS: *m/z* 364.5 $[M]H^+$, 402.7 $[M]K^+$.

2.2.2. Synthesis of PEG-monoAlkyne (6)

PEG_{2000} (**4**) (500 mg, 0.25 mmol) and pentynoic anhydride (**5**) (37 mg, 0.2 mmol, 1 equiv) were dissolved in 15 mL DCM in the presence of triethylamine (33 mg, 0.32 mmol, 1.3 equiv) and DMAP (40 mg, 0.32 mmol, 1.3 equiv). The reaction mixture was stirred at rt for 24 h, followed by extraction two times with ultrapure water. The organic phases were combined, dried over anhydrous sodium sulfate and evaporated, leading to PEG-monoAlkyne (**6**) as a white solid. Sample (**6**) was directly used in the next synthetic step, without further purification. Peaks integration pointed out that the sample is a mixture of PEG-monoAlkyne (**6**) and unreacted PEG diol (**4**) (7:3 ratio, the latter removed in the next synthetic step and related work up). ^{1}H NMR (500 MHz, $CDCl_3$) δ: 4.25 (t, $J = 5.3$ Hz, 2H, CH_2), 3.60–3.72 (m, CH_2CH_2O), 2.57–2.60 (m, 2H, CH_2), 2.48–2.51 (m, 2H, CH_2), 1.99 (s, 1H, CH).

2.2.3. Synthesis of PLA-PEG-alkyne (8)

The mixture obtained in the previous step (containing 75 mg of PEG-monoAlkyne, 0.036 mmol) was dissolved in 20 mL of DCM together with EDCI (10 mg, 0.054 mmol, 1.5 equiv), DMAP (2.4 mg, 0.02 mmol, 0.5 equiv) under inert atmosphere; commercial PLA (**7**) (565 mg, 0.054 mmol; 1.5 equiv) was added dropwise and the reaction mixture was stirred for 48 h at room temperature. The solution was washed with small volumes of ultrapure water three times, the organic phases were combined, dried over anhydrous sodium sulfate and concentrated under vacuum. PLA-PEG-alkyne (**8**) was washed with DCM/cold methanol and recovered after centrifugation as a white solid (232 mg, 55%). ^{1}H NMR (500 MHz, $CDCl_3$) selected peaks δ: 5.19 (m, $[CH]_n$ PLA), 4.30 (m, 2H, CH_2), 4.25 (m, 2H, CH_2), 3.63–3.65 (m, CH_2CH_2O), 2.58–2.60 (m, 2H, CH_2), 2.49–2.51 (m, 2H, CH_2), 1.98 (s, 1H, CH), 1.56 (m, $[CH_3]_n$ PLA).

2.2.4. Synthesis of PLA-PEG-NAC (9)

PLA-PEG-monoalkyne (**8**) (800 mg, 0.06 mmol) and NAC-azide (**3**) (65 mg, 0.18 mmol, 3 equiv) were dissolved in 5 mL of anhydrous DMF; $CuSO_4$ (29 mg, 0.16 mmol, 3 equiv) and sodium ascorbate (76.5 mg, 0.36 mmol, 6 equiv) were added and the reaction mixture was stirred for 72 h at rt. After removal of the organic solvent, the residue was washed three times with ultrapure water (3 x 40 mL) and the suspension was centrifuged (20 min, 13000 rpm). The residue was freeze-dried yielding PLA-PEG-NAC (**9**) (490 mg, 62%) as a white solid. ^{1}H NMR (500 MHz, $CDCl_3$) selected peaks δ: 7.34 (s, 1H, H5-triazole), 5.19 (m, $[CH]_n$ PLA), 4.51–4.48 (m, 2H, CH_2), 4.31–4.27 (m, 2H, CH_2), 4.27–4.25 (m, 2H, CH_2), 3.68–3.58 (m, CH_2CH_2O), 3.03 (m, 2H, CH_2), 2.49–2.51 (m, 2H, CH_2), 1.99 (s, 3H, CH_3), 1.56 (m, $[CH_3]_n$ PLA).

2.2.5. Synthesis of crotonyl-amide-BODIPY (12)

In a two-neck flask, amino-BODIPY (**11**) (50 mg, 0.15 mmol) was dissolved in 5 mL of anhydrous DCM in an inert atmosphere; triethylamine (17 mg, 0.17 mmol, 1.1 equiv) and crotonyl chloride (**10**) (18 mg, 0.17 mmol, 1.1 equiv) were added, protected from light using aluminum foil. The reaction mixture was stirred for 72 h at rt, followed by extraction with saturated sodium bicarbonate solution (2 x 5 mL); the organic phase was dried over anhydrous sodium sulfate and evaporated under reduced pressure. The crude was purified by column chromatography using silica as the stationary phase and a gradient mixture of hexane/EtOAc (80:20, then 70:30) as the eluent to obtain crotonyl-amide-BODIPY (**12**) (36 mg, 58%). ^{1}H NMR (500 MHz, $CDCl_3$) δ: 7.72 (d, $J = 8.3$ Hz, $2H_{(Z)}$), 7.68 (d, $J = 8.5$ Hz, $2H_{(E)}$), 7.41 (sb, NH), 7.23 (d, $J = 8.4$ Hz, $4H_{(E+Z)}$), 7.06–7.02 (m, $1H_{(Z)}$), 6.09–5.97 (m, $1H_{(E)}$), 5.97 (s, $4H_{(E+Z)}$), 5.40–5.36 (m, $2H_{(E+Z)}$), 3.22 (d, $J = 7.2$ Hz, $3H_{(E)}$), 2.55 (s, $12H_{(E+Z)}$), 1.94 (dd, $J = 6.9, 1.7$ Hz, $3H_{(Z)}$), 1.42 (s, $12H_{(E+Z)}$). ESI-MS: m/z 388.3 $[M-Fluorine]^+$ and 408.4 $[M]H^+$.

2.2.6. Labelling reaction of PLA-PEG-NAC (9) with crotonyl-amide-BODIPY (12)

To confirm the presence of sulfhydryl-reactive chemical groups on PLA-PEG-NAC (**9**), a typical thiol-ene coupling reaction was performed with crotonyl-amide-BODIPY (**12**) in DMF. Briefly, 2.1 mg ($1.18 * 10^{-7}$ mmol) of PLA-PEG-NAC (**9**) was added to a DMF solution (0.6 mL) of 2.2 mg ($4.9 * 10^{-6}$ mmol) of crotonyl-amide-BODIPY (**12**) and stirred at 50°C for 14 h. The solution was poured in 20 mL of diethylether. The precipitate was washed several times with diethylether in an ultrasonic bath (the solution was tested by UV–vis to verify the absence of BODIPY derivative). The solid fraction was collected and dried in vacuum for 24 h at 50°C to obtain PLA-PEG-NAC-BODIPY (**13**).

2.3. Nanoformulation of PLA-PEG-NAC and characterization

2.3.1. Preparation of PLA-PEG-NAC@LNZ NPs

PLA-PEG-NAC@LNZ NPs were prepared at 10:5 polymer:drug ratio. LNZ (15 mg) and PLA-PEG-NAC (30 mg) were dissolved in 1.5 ml of DMSO. After a brief sonication, the organic solution was added dropwise into 23 mL of ultrapure water under stirring, leading to the formation of a suspension. After 4 h of stirring, the suspension was transferred into a dialysis membrane (3.5–5 KDa) previously conditioned in water for 10 min. The sealed dialysis tube was plunged in 500 ml of ultrapure water and kept under gentle stirring. The entire volume of water was replaced after 3 h, after 15 h 30 min, after 19 h 30 min. The final suspension was lyophilized, yielding PLA-PEG-NAC@LNZ NPs as a white powder (22 mg). Similarly, "empty" PLA-PEG-NAC NPs were prepared using the same method without the drug and used as controls.

2.3.2. Preparation of PLA-PEG-NAC@Pent NPs

Pent free base, used for drug encapsulation, was obtained from Pent isethionate salt as follows: 100 mg of pentamidine isethionate was dissolved in 3 mL of ultrapure water under stirring. A cold solution of NaOH was gradually added until the pH of the solution was adjusted to 12. The solution was then refrigerated overnight, centrifuged at 10000 rpm for 5 min and washed twice with ultrapure water to obtain Pent free base as a white powder. The product was freeze-dried and stored in the fridge. PLA-PEG-NAC@Pent NPs were prepared at 10:3 polymer:drug ratio. Pent free base (9 mg) and PLA-PEG-NAC (30 mg) were dissolved in 3 ml of DMSO. After a brief sonication, the organic solution was added dropwise into 20 mL of stirring ultrapure water with the formation of a suspension. After 4 h of stirring, the suspension was transferred into a dialysis membrane (3.5–5 KDa) previously conditioned in water for 10 min. The sealed dialysis tube was plunged in 500 ml of ultrapure water and kept under gentle stirring. The entire volume of water was replaced after 3 h and after 19 h. The final suspension was lyophilized, yielding PLA-PEG-NAC@Pent NPs (18 mg) as a white powder.

2.3.3. Size and ζ potential

DLS and ζ-potential measurements were carried out on lyophilized PLA-PEG-NAC@LNZ NPs, PLA-PEG-NAC@Pent NPs and empty PLA-PEG-NAC NPs after resuspension in ultrapure water (concentration 0.05 mg/mL) and sonication (15 min).

2.3.4. Determination of drug loading and encapsulation efficiency

The drug content in the NPs and the loading efficiency were determined by UV–Vis spectroscopy by dissolving a weighted amount of NPs in 2 mL of methanol. The amount of encapsulated drug was calculated at the wavelength of 257 nm for LNZ or 265 nm for Pent. A calibration curve for LNZ and for Pent free base in methanol was previously constructed using the concentration range 3.4–34 μg/mL (10.2 μM −102.0 μM) for LNZ and 0.6–22.0 μg/mL (1.8 μM-65 μM) for Pent free base. A molar extinction coefficient of $\varepsilon \cong 19407\ M^{-1}\ cm^{-1}$ for LNZ and $\varepsilon \cong 28794\ M^{-1}\ cm^{-1}$ for Pent free base in methanol was calculated. Drug incorporation was expressed in terms of drug loading (DL) and encapsulation efficiency (EE) as follows:

$$- DL\ (\%) = [Mass\ of\ drug\ (mg)\ incorporated\ in\ the\ NPs / Mass\ of\ drug - loaded\ NPs\ (mg)]\ x\ 100$$

– $EE\ (\%) = [Mass\ of\ drug\ (mg)\ incorporated\ in\ the\ NPs / Total\ mass\ of\ drug\ (mg)\ used\ in\ the\ formulation] \times 100$

2.3.5. Drug release studies

Drug release from PLA-PEG-NAC NPs was studied using a dialysis method. PLA-PEG-NAC@LNZ NPs (0.42 mg/mL, containing 16 μg LNZ based on the DL value) or PLA-PEG-NAC@Pent NPs (0.71 mg/mL, containing 32 μg Pent based on the DL value) were dispersed in PBS (0.01 M, pH 7.4), sonicated for 15 min and transferred into the dialysis membrane (MWCO 3.5–5 kDa, Spectra/Por®) that was then immersed in a beaker containing 5 mL PBS. The temperature was set at 37°C and the release experiment was continued for 72 h. Aliquots of the release medium (1 mL) were withdrawn for analysis at different time intervals (1 h, 2 h, 4 h, 6 h, 8 h, 24 h, 48 h, 72 h) and replaced with an equal volume of fresh buffer. The absorbance of collected samples was analyzed at λ_{max} 251 nm and 261 nm for LNZ and Pent, respectively, to quantify the released drug. A calibration curve in PBS was previously constructed for LNZ, Pent free base, and Pent isethionate in the concentration range 0.34–25 μg/mL, 2.2–28 μg/mL and 1.25–30 μg/mL, respectively. The following molar extinction coefficient values for LNZ, Pent free base, and Pent isethionate in PBS were obtained: $\varepsilon_{251nm} \cong 18486\ M^{-1}\ cm^{-1}$, $\varepsilon_{261nm} \cong 23547\ M^{-1}\ cm^{-1}$, $\varepsilon_{262nm} \cong 25070\ M^{-1}\ cm^{-1}$. The release profile of free LNZ and free Pent in PBS was also investigated at the same concentration and experimental conditions as the drug-loaded NPs.

2.4. Cell cytotoxicity

2.4.1. Cell culture

Vero cells (African green monkey kidney epithelial cells) were maintained in Dulbecco's Modified Eagle Medium (DMEM) supplemented with 10% heat-inactivated fetal bovine serum (FBS), 1% L-glutamine, and 1% penicillin–streptomycin. Cells were cultured at 37 °C in a humidified incubator with 5% CO_2 and routinely passaged at 70–80% confluence using trypsin–EDTA.

2.4.2. MTT assay

Cell metabolic activity was evaluated by MTT assay which is based on the reduction of a tetrazolium salt to a coloured formazan product by metabolically active cells. The assay was performed using a commercially available kit, following the manufacturer's instructions. Briefly, Vero cells were seeded in 96-well plates at a density of 5×10^4 cells per well in 180 μL of complete medium and allowed to adhere overnight. After incubation, cells were treated with PLA-PEG-NAC@LNZ NPs, PLA-PEG-NAC@Pent NPs (drug concentration 1–16 μg/mL), empty PLA-PEG-NAC NPs (at the same polymer concentration used for testing drug-loaded NPs) and further incubated for 24 h. At the end of the treatment, MTT reagent solution was added to each well, and the plates were incubated for 3 h at 37°C. Following incubation, MTT solvent was added to dissolve the formazan crystals. Absorbance was then measured at 590 nm using a microplate reader. After subtraction of the background signal attributable to the culture medium, the data were normalized to the untreated control to assess the cytotoxic effect of the treatment according to the following relationship:

$$[100 \times (control - sample)]/control$$

The percentage of viable cells was then determined as the complement of cytotoxicity.

2.5. Microbiology

2.5.1. Minimal inhibitory concentration and minimal bactericidal concentration

The bacteria used in this study were *Staphylococcus aureus* ATCC 6538, methicillin-resistant *S. aureus* (MRSA) ATCC 43300, *S. epidermidis* ATCC 35984 and *Enterococcus faecium* (VREfm) DSM 17050. Minimal inhibitory concentration (MIC) and minimal bactericidal concentration (MBC) of the PLA-PEG-NAC@LNZ NPs (containing 32 μg LNZ in 800 μg of NPs, based on DL value), LNZ and empty PLA-PEG-NAC NPs were performed according to the guidelines of the Clinical and Laboratory Standards Institute (CLSI) [17] with some modifications. The samples were twofold diluted in 96-well round-bottomed using cation-adjusted Muller-Hinton broth (CAMHB) and overnight bacterial cultures were inoculated to yield a final concentration of 5×10^5 CFU/mL. The MIC was considered as the lowest concentration of each sample giving a complete inhibition of visible microbial growth after incubation for 18–24 h. In order to confirm MIC values, 2,3,5-triphenyltetrazolium chloride (TTC) 0.125% (w/v) was added in all the wells, followed by 1 h of incubation. The TTC is a tetrazolium salt widely used in the MIC determination and is a colorless compound when solubilized with water, however in the presence of metabolically active bacteria is reduced to red-colored formazan which is directly proportional to the quantity of viable cells. The MBC was determined by seeding 20 μL from all clear wells onto Muller-Hinton agar (MHA) and incubated at 37°C for 24 to 48 h. The MBC was defined as the lowest concentration which killed 99.9% of the inoculum. The data from at least three replicates were evaluated and modal results were calculated.

2.5.2. Effect of PLA-PEG-NAC@LNZ NPs on biofilm formation

The effect of PLA-PEG-NAC@LNZ NPs, free LNZ and empty PLA-PEG-NAC NPs on biofilm-forming ability of *S. aureus* (MRSA) ATCC 43300 was tested on polystyrene, flat-bottomed microtiter plates, as previously described [18]. An overnight culture in TSB + 1% glucose (TSBG) was adjusted to 1×10^6 CFU/mL and dispensed into each well of 96-well polystyrene flat-bottomed microtiter plates containing twofold serial dilutions of the samples in order to obtain the final concentration equal to 5×10^5 CFU/mL. After incubation at 37 °C for 24 h, the planktonic phase was removed and each well was washed twice with sterile PBS (pH 7.4), dried, stained for 1 min with 0.1% safranin and washed with water. The stained biofilm biomass was re-suspended in 30% (v/v) acetic acid and absorbance at 490 nm ($Abs_{490\ nm}$) was measured using a spectrophotometer EIA reader. A biofilm control consisting of a TSBG medium was included.

The reduction percentage of the biofilm biomass was calculated using the following equation:

$$100 - (mean\ Abs_{490\ nm}\ of\ sample / mean\ Abs_{490\ nm}\ of\ control\ well) \times 100$$

2.5.3. Fluorescence microscopy

Biofilm viability was evaluated using the LIVE/DEAD BacLight Viability Kit (Molecular Probes). Thebiofilm formation assay was performed as described above, using black microtiter plates with a glass bottom. After treatment with sub-MIC concentrations of PLA-PEG-NAC@LNZ NPs, free LNZ and empty PLA-PEG-NAC NPs, the biofilms were washed and stained with 1 mL of a SYTO 9/propidium iodide (PI) solution (1:1). Plates were incubated at room temperature for 15 min in the dark. Subsequently, excess stain was removed, and samples were observed using an inverted microscope Axio Observer.Z1 equipped with an Apotome 3 and images were acquired with ZEN 3.12 software.

2.5.4. Effect of PLA-PEG-NAC@LNZ NPs on biofilm-embedded MRSA

Effect of PLA-PEG-NAC@LNZ NPs on early (8 h) and late (24 h) preformed MRSA biofilm was evaluated by colorimetric and metabolic viability (XTT) assays as previously reported [11,19]. Overnight cultures of MRSA ATCC 43300 in TSBG were adjusted to 1×10^6 CFU/mL and 100 μL were added to each well of a polystyrene flat bottomed 96-microtitre plate. The plates were incubated at 37 °C for 24 h. After incubation, the supernatant was removed and biofilms were carefully washed twice with sterile PBS. Biofilms were treated with 100 μL of PLA-PEG-NAC@LNZ NPs at 8 x MIC and 4 x MIC, free LNZ at 8 x MIC and 4 x

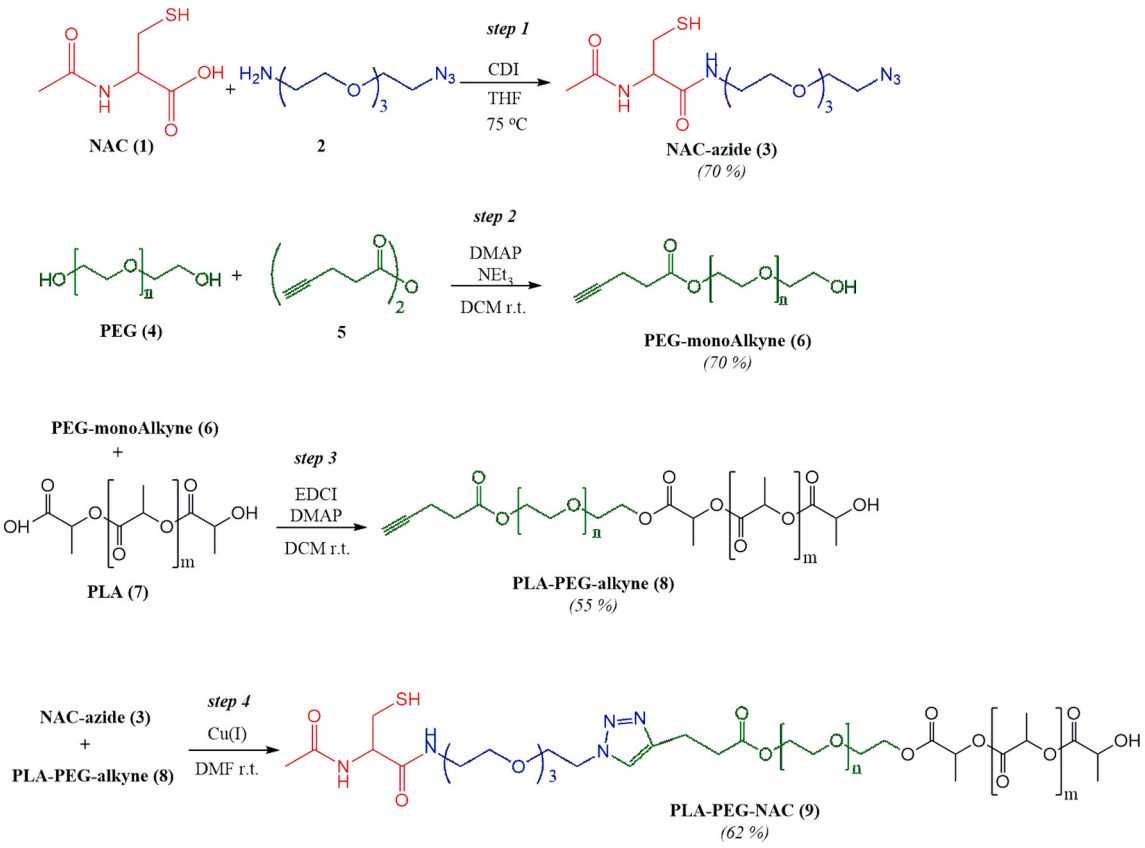

Scheme 1. Step-by-step synthesis of PLA-PEG-NAC (**9**) and its intermediates: NAC-azide (**3**), PEG-monoAlkyne (**6**), PLA-PEG-alkyne (**8**).

MIC and empty PLA-PEG-NAC NPs or medium (control) for 24 h at 37 °C. To verify the activity on biofilm biomass and cell metabolic viability, the supernatant was removed and biofilms were washed twice with PBS before being:

1. Dried, stained for 1 min with 0.1% safranin and resuspended in 30% (v/v) acetic acid for Abs_{490} evaluation.
2. Exposed to a Cell Proliferation Kit II XTT (Roche Diagnosis, Mannheim, Germany), as previously reported. This assay utilizes the reduction of a tetrazolium salt (2,3-bis[2-methyloxy-4-nitro-5-sulfophenyl]–2H-tetrazolium-5-carboxanilide (XTT)) by metabolically active cells to a colored water-soluble formazan derivative that can be easily quantified colorimetrically. A decrease in the number of live cells correlates with a decrease in overall activity of the dehydrogenases responsible for transforming the sodium salt of tetrazolium XTT into formazan. Specifically, a saline solution containing XTT (final concentration 0.3 mg/mL) for 5 h at 37°C and then formazan was quantified spectrophotometrically at 490 nm. Data were obtained from at least three independent experiments performed in duplicate.

The reduction percentage of biofilm biomass/metabolic activity was calculated using the above mentioned equation.

2.5.5. Checkerboard test

The checkerboard test was carried out to determine the potential synergistic, additive, or even antagonistic effects of combinations of free LNZ with free Pent and of PLA-PEG-NAC@LNZ NPs with PLA-PEG-NAC@Pent NPs against *E. coli* ATCC 10536. Dilutions of the combinations, from 2 x MIC to the serial dilution below, were inoculated in microtiter plates and incubated as described above [20]. The checkerboard test was used as the basis to calculate a Fractional Inhibitory Concentration (FIC) according to the formulas: $FIC_A = MIC_{A+B}/MIC_A$, $FIC_B = MIC_{B+A}/MIC_B$, FIC Index = $FIC_A + FIC_B$. The MIC_{A+B} value is the MIC of compound A in the presence of compound B, and vice versa for MIC_{B+A}. FIC Index (FICI) values were interpreted as follows: synergistic effect for FICI $\leq$ 0.5; additive effect for FICI $>$ 0.5–1; indifference for FICI $>$ 1 to $<$ 2; and antagonism for FICI $\geq$ 2 [21]. All experiments were performed in triplicate. The results were also reported as isobolograms, constructed by plotting the best concentrations.

2.6. Statistical analysis

Results, expressed as the mean value ± standard deviation, were statistically analyzed using the software GraphPad Prism 10.6.1 developed by GraphPad Software Inc. (San Diego, CA, USA). A one-way analysis of variance (ANOVA) was used to determine significant differences among the samples and the intreated control. Multiple comparisons were performed among groups by the Tukey's test. The results with a p-value < 0.05 were considered statistically significant.

3. Results and discussion

3.1. Chemistry

The synthesis of the novel N-acetylcysteine conjugated with PLA-PEG copolymer (PLA-PEG-NAC) was achieved by a multistep pathway (Scheme 1). Chemoselectivity and orthogonality are crucial in both polymer synthesis and functionalization for providing access to multifunctional architectures with specific structures and properties that can be eventually formulated into nanoparticles. Therefore, suitable building blocks (*i.e.,* NAC-azide and PLA-PEG-alkyne) were first synthesized by combining amide coupling and esterification reactions; afterwards the copper-catalyzed azide-alkyne Huisgen cycloaddition (CuAAC) yielded the covalent conjugation of NAC to the amphiphilic copolymer PLA-PEG. Overall, these synthetic methods proved to be powerful tools

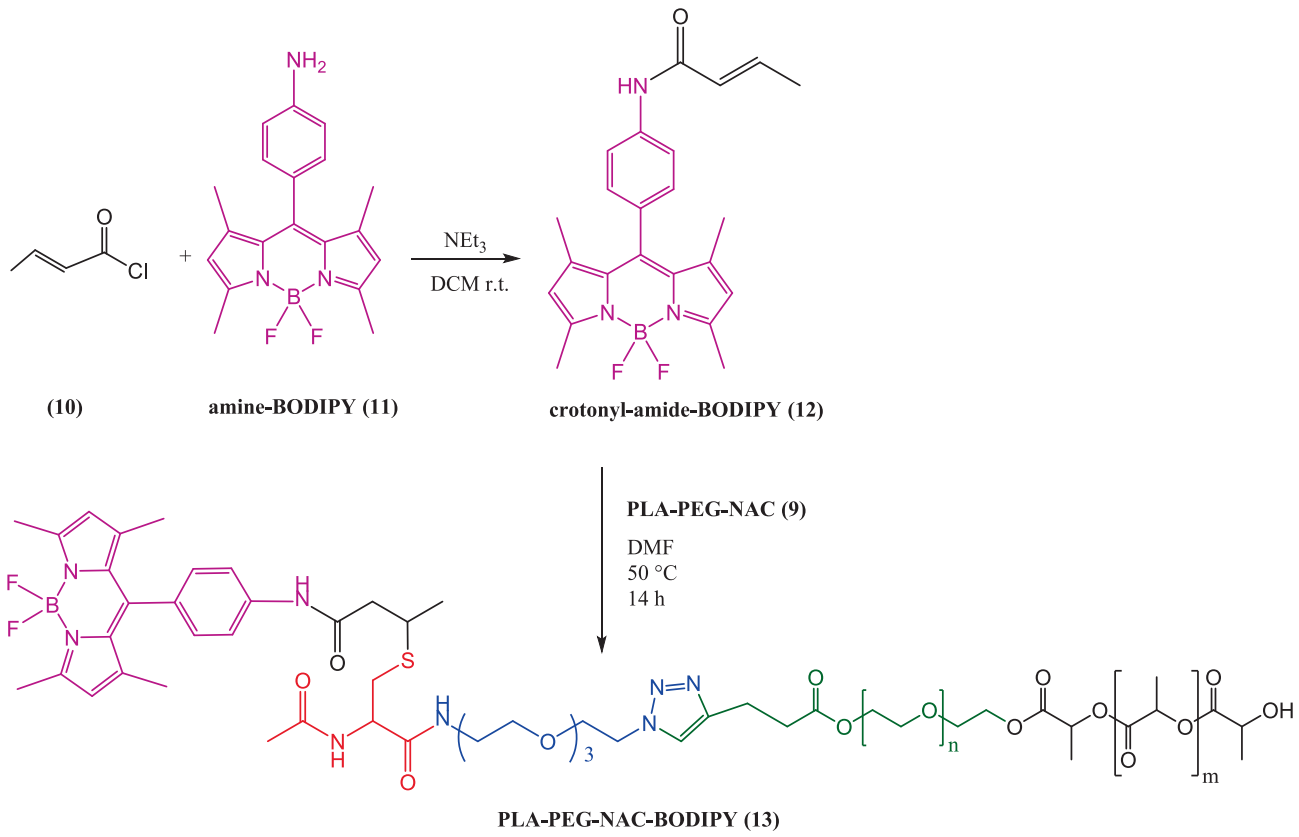

Scheme 2. Synthetic pathway for PLA-PEG-NAC-BODIPY (**13**) starting from PLA-PEG-NAC (**9**) and crotonyl-amide-BODIPY (**12**).

in polymer organic chemistry due to their high conversion efficiency, mild reaction conditions, and compatibility with bioactive compounds [22–24]. Specifically, NAC-azide (**3**) was synthesized by conjugation of NAC (**1**) with 11-azido-3,6,9-trioxaundecan-1-amine (**2**), selected as bifunctional linker and suitable spacer to ensure optimal grafting between the bioactive molecule NAC and the functional end-groups of the polymer (Scheme 1, *step 1*). The chemical structure of NAC-azide (**3**) was confirmed by one- and two-dimensional NMR analyses, FT-IR, and mass spectrometry (Figs. S1-S5). The comparison between ^{1}H NMR spectra of NAC-azide (**3**) and the starting products, NAC (**1**) and 11-azido-3,6,9-trioxaundecan-1-amine (**2**), confirmed the success of the coupling reaction. Specifically, an evident shift of diagnostic peaks was observed, including the amine methylene protons of the linker, becoming amidic, from 2.78 to 3.15 ppm, the resonance relative to the methine proton of NAC from 4.60 to 4.55 ppm, and the methylene protons of NAC side chain from 2.86 and 2.95 ppm to 3.32 and 3.03 ppm, respectively (Fig. S1). Moreover, ^{13}C NMR spectrum of NAC-azide (**3**) (Fig. S2) confirmed the presence of the new amidic bond at 175.59 ppm along with the resonance at 171.57 ppm attributed to the N-acetyl moiety. The complete assignment of signals was accomplished by gCOSY and gHSQCAD analyses (Figs. S3-S4). The structure of NAC-azide (**3**) was also confirmed by mass spectrometry analysis, showing peaks at *m/z* 364.5 $[M]H^{+}$ and 402.7 $[M]K^{+}$ (Fig. S5).

In parallel, a clickable PLA-PEG-alkyne (**8**) was obtained by mono-alkynylation of commercial PEG_{2000} (**4**) with pentynoic anhydride (**5**) in the presence of DMAP and triethylamine (Scheme 1, *step 2*) followed by esterification of the terminal hydroxyl group of PEG-monoAlkyne (**6**) with PLA (**7**) (Scheme 1, *step 3*). The mono-alkynylation of PEG was confirmed by ^{1}H NMR analysis (Fig. S6) by the appearance of the typical signal corresponding to the methylene ester protons at 4.25 ppm together with the set of signals related to the pentynoic moiety (1.99, 2.48 and 2.57 ppm). Nevertheless, peak integration pointed out that the sample was a mixture of PEG-monoAlkyne (**6**) and unreacted PEG diol

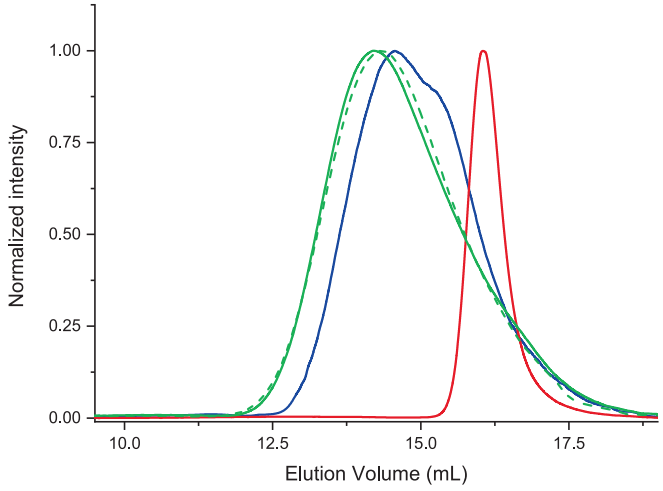

Fig. 2. GPC traces, using differential refractometer as detector, of commercial PLA (**7**, blue line), PEG-monoAlkyne (**6**, red line), and PLA-PEG-NAC-BODIPY (**13**, solid green line); trace of PLA-PEG-NAC-BODIPY (**13**) using UV–visible detector fixed at 502 nm (dashed green line).

(**4**) (7:3 ratio), in good agreement with reported data [25]. The PEG diol was removed in the next synthetic step and related work up (see Experimental), as already reported for other PEG mono-functionalizations [26]. The IR spectrum of (**8**) confirmed the presence of the alkyne group at 2108 cm^{-1} (Fig. S7) although the peak intensity was small, as expected, due to the dominant peaks from the polymer.

Finally, the CuAAC between NAC-azide (**3**) and PLA-PEG-alkyne (**8**) was accomplished in the presence of $CuSO_4$ and sodium ascorbate,

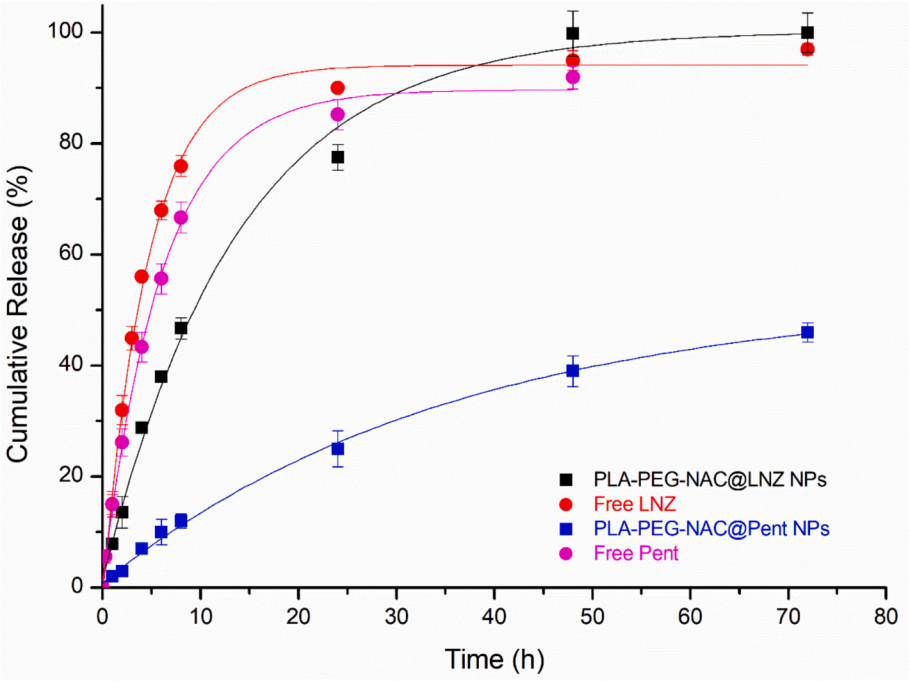

Fig. 3. Cumulative percentage release of free drugs (LNZ and Pent) and drugs from PLA-PEG-NAC@LNZ NPs and PLA-PEG-NAC@Pent NPs *vs* time, assessed in PBS (pH 7.4) at 37°C by dialysis method. Data are reported as the mean ± SD (n = 3). The curves were fitted using the first order mathematical model (simple exponential).

leading to PLA-PEG-NAC (**9**) (Scheme 1, *step 4*).

NMR analysis was inconclusive in confirming the covalent grafting of NAC to the polymer end-group, as expected, due to the relatively low amount of NAC present (about 10 μg/mg). However, IR spectroscopy attested for the conversion of the alkyne (**8**) and azide (**3**) into the triazole derivative (**9**) by monitoring the disappearance of both the alkyne's characteristic C≡C stretch (2108 cm^{-1}) and the N=N=N stretching vibration at 2099 cm^{-1} (Fig. S7).

To confirm the covalent grafting of NAC to the PLA-PEG copolymer, a typical thiol-ene labelling reaction was performed between PLA-PEG-NAC (**9**) and a novel crotonyl-amide-BODIPY (**12**). The latter was newly synthesized by conjugation between crotonyl chloride (**10**) and amine-BODIPY (**11**) (Scheme 2) and characterized by ^{1}H NMR and mass spectrometry analysis (Fig. S8-S9). The thiol-ene Michael addition was performed by reacting crotonyl-amide-BODIPY (**12**) with PLA-PEG-NAC (**9**) in DMF at 50 °C for 14 h [27] producing PLA-PEG-NAC-BODIPY (**13**) (Scheme 2). Fig. 2 reports the GPC traces of PLA (blue line), PEG-monoAlkyne (red line) and PLA-PEG-NAC-BODIPY (green lines). Specifically, the BODIPY-labelled PLA-PEG-NAC sample, analyzed with refractive index and UV–Vis detectors (Fig. 2, solid and dashed green lines, respectively) connected in parallel, revealed a signal at the absorption maximum of BODIPY (λ_{max} = 502 nm) that partially overlapped with the corresponding refractive index signal, confirming the presence of the sulfhydryl-reactive end-group on the polymeric structure.

3.2. Nanoantibiotics formulation and characterization

The intrinsic self-assembly ability of amphiphilic PLA-PEG-NAC was exploited to produce nanoparticles for encapsulation of LNZ and Pent. The aminoacid-polymer conjugate was proven effective in forming drug-loaded NPs. The technical optimization in terms of drug/polymer ratio and loading conditions was adjusted to favor drug incorporation and to maximize drug loading while maintaining nanoparticle stability and reproducibility. Specifically, PLA-PEG-NAC@LNZ NPs and PLA-PEG-NAC@Pent NPs were formulated by dialysis (Fig. 1B), the latter being selected based on our previous comparative studies on PLA-PEG nanoformulation methods [11].

Briefly, polymer and drug were solubilized in DMSO and added dropwise into stirring water; the resulting suspension was placed inside a suitable dialysis membrane to promote the diffusion out of organic solvent and excess of drug. PLA-PEG-NAC@LNZ and PLA-PEG-NAC@Pent Nanoantibiotics were assessed in terms of particle size, surface charge, encapsulation efficiency (EE) and drug loading (DL) capacity. Mean particle hydrodynamic diameter (D_H) was about 246 nm and 231 nm for PLA-PEG-NAC@LNZ and PLA-PEG-NAC@Pent NPs, respectively, and 229 nm for empty NPs. The ζ potential values were observed to be −26, −25 and −28 mV, respectively, attesting for a good colloidal stability without sedimentation along the time. The encapsulation efficiency was 12% for LNZ and 20% for Pent with a drug loading capacity of 4% and 4.5%, respectively. The modest EE is consistent with the physicochemical properties of both drugs since LNZ possesses some water solubility and Pent is a relatively hydrophilic molecule; therefore, they typically exhibit moderate affinity for hydrophobic polymer matrices. The relatively low EE values were inherent to our focus on maximizing DL rather than optimizing EE. To this end, we investigated formulation protocols employing higher polymer:drug ratios (10:3 and 10:5 w/w, see Experimental), which resulted in increased drug content. Lower polymer:drug ratios, which may potentially enhance EE, were not explored at this stage, representing an important direction for greater clinical relevance in future optimization.

Drug release studies were conducted at physiological pH using the dialysis method. Cumulative percentage release values of LNZ and Pent from PLA-PEG-NAC NPs over 72 h were reported in Fig. 3 together with the release profile of free drugs under the same conditions, for comparison. Free LNZ and free Pent rapidly diffused across the dialysis membrane with 56% of LNZ and 43% of Pent released within the initial 4 h. The diffusion of both drugs was more than 80% in the first 24 h and almost complete within 72 h. Compared to the control data, the release of both drugs from NPs appeared sustained and prolonged, as typically expected and desirable for nanoparticles-based drug delivery system, designed to act as a drug *"reservoir"*. Specifically, approximately 30% of LNZ was released from PLA-PEG-NAC@LNZ NPs at a relatively rapid

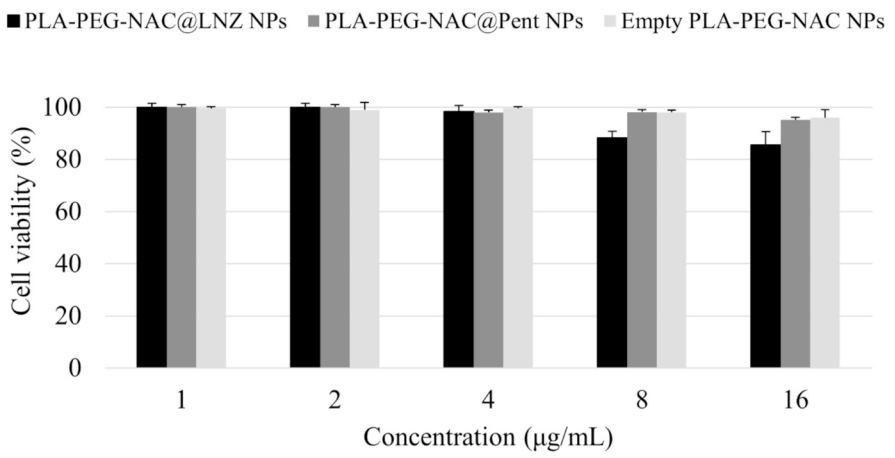

Fig. 4. Cell viability. MTT assay on VERO cells treated with PLA-PEG-NAC@LNZ NPs and PLA-PEG-NAC@Pent NPs at different concentration of LNZ or Pent (1–16 μg/mL). Empty PLA-PEG-NAC NPs were tested at the same polymer concentration used for testing drug-loaded NPs.

rate during the first 4 h (burst phase), followed by slower release rate prolonged over the next hours (about 50% in 8 h, 78% in 24 h, completed in around 48 h). An overall slower release profile was observed for Pent from PLA-PEG-NAC@Pent NPs with only 7% of drug released in the first 4 h, about 12% in 8 h, 25% in 24 h, reaching 46% within 72 h. The initial release is commonly ascribed to the drug detachment from NPs surface while the later sustained profile is related to the release from the inner core mainly due to the drug diffusion and/or polymer matrix erosion. In drug delivery systems, release profiles can be governed by different mechanisms, including simple diffusion, erosion, degradation, and absorption processes. To better understand these phenomena and accurately predict release kinetics and material interactions, several mathematical models have been proposed in literature [28].

In the present study, a first-order mathematical model (simple exponential) was applied to fit the drug release data. This approach was used to evaluate the kinetic profiles of drugs released from PLA-PEG-NAC@LNZ NPs and PLA-PEG-NAC@Pent NPs, as well as from the corresponding free drugs (Fig. 3). A correlation coefficient (R^2) of about 0.99 was obtained for all samples (Table S1) indicating appropriate fitting of the model to the experimental data. These results suggest that drug release from nanoparticles is primarily governed by simple diffusion, which depends on both drug concentration and the composition/morphology of the delivery system. This behavior is consistent with nanosystems acting as *"drug reservoirs"* embedded within a homogeneous polymeric matrix, where diffusion is controlled by a constant coefficient.

A similar mechanism was observed for the release of free drugs, which diffuse through the semi-permeable membrane used in the release experiments. The parameter values (R^2 and K) obtained from fitting the experimental data to a first-order model are summarized in Table S1.

Overall, the conjugation of polymers with cysteine derivatives significantly modulated drug release and drug permeation with a different effect on LNZ and Pent likely due to their different chemical-physical features and solubilities.

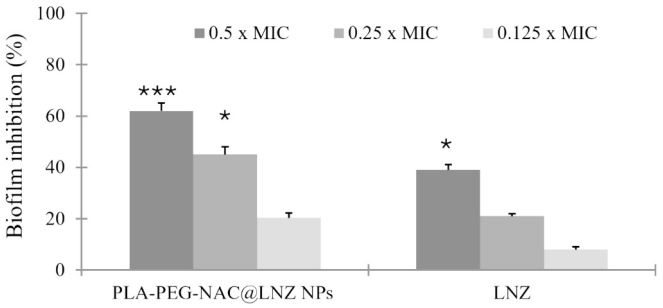

Fig. 5. Inhibition of *S. aureus* MRSA ATCC 43300 biofilm formation in the presence of sub-MICs of PLA-PEG-NAC@LNZ NPs and free LNZ. Values are expressed as mean ± standard deviation of biofilm inhibition (%). Pairwise comparisons with the control (Tukey's test) are indicated as follows: * ($p < 0.05$); *** ($p < 0.001$).

3.3. Cell cytotoxicity

MTT assay on Vero cells demonstrated no notable toxicity of PLA-PEG-NAC NPs (Fig. 4), either in their drug-loaded or unloaded forms, with cell viability remaining above 80% even at the highest tested concentration (16 μg/mL).

3.4. Microbiological studies

The antimicrobial features of PLA-PEG-NAC@LNZ NPs were evaluated by the assessment of their MIC and MBC values against *S. aureus*, MRSA, *S. epidermidis* and VREfm strains, their effect on biofilm formation and on early (8 h) and late (24 h) preformed MRSA biofilm. Furthermore, the efficacy of PLA-PEG-NAC@LNZ NPs in combination with PLA-PEG-NAC@Pent NPs against *E. coli* was investigated.

MIC values of PLA-PEG-NAC@LNZ NPs were reported in Table 1. The activity of LNZ embedded into our polymeric NPs resulted in MIC and MBC values of 2 μg/mL and 16 μg/mL, respectively. Although the

Table 1
Antibacterial activity of free LNZ, PLA-PEG-NAC@LNZ NPs expressed as LNZ concentration (μg/mL) and empty PLA-PEG-NAC NPs.

Samples	*S. aureus* ATCC 6538		*S. aureus* (MRSA) ATCC 43300		*S. epidermidis* ATCC 35984		*E. faecium* (VRE) DSM 17050	
	MIC	MBC	MIC	MBC	MIC	MBC	MIC	MBC
Free LNZ	2	16	2	16	1	16	2	16
PLA-PEG-NAC@LNZ	2	16	2	16	2	16	2	16
PLA-PEG-NAC	>16	>16	>16	>16	>16	>16	>16	>16

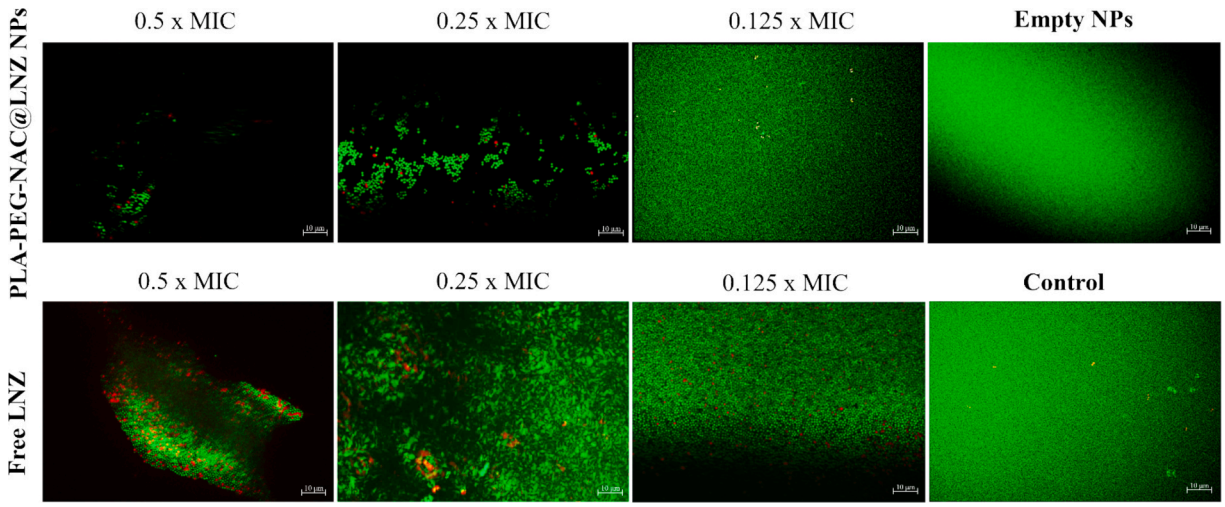

Fig. 6. Representative fluorescence images of *S. aureus* (MRSA) biofilm formation in the presence of PLA-PEG-NAC@LNZ NPs and free LNZ. The viable cells are green (SYTO 9) and dead cells are red (propidium iodide, PI). Images observed with inverted microscope Axio Observer.Z1 equipped with an Apotome 3 and acquired with ZEN 3.12 software. Magnification 100X.

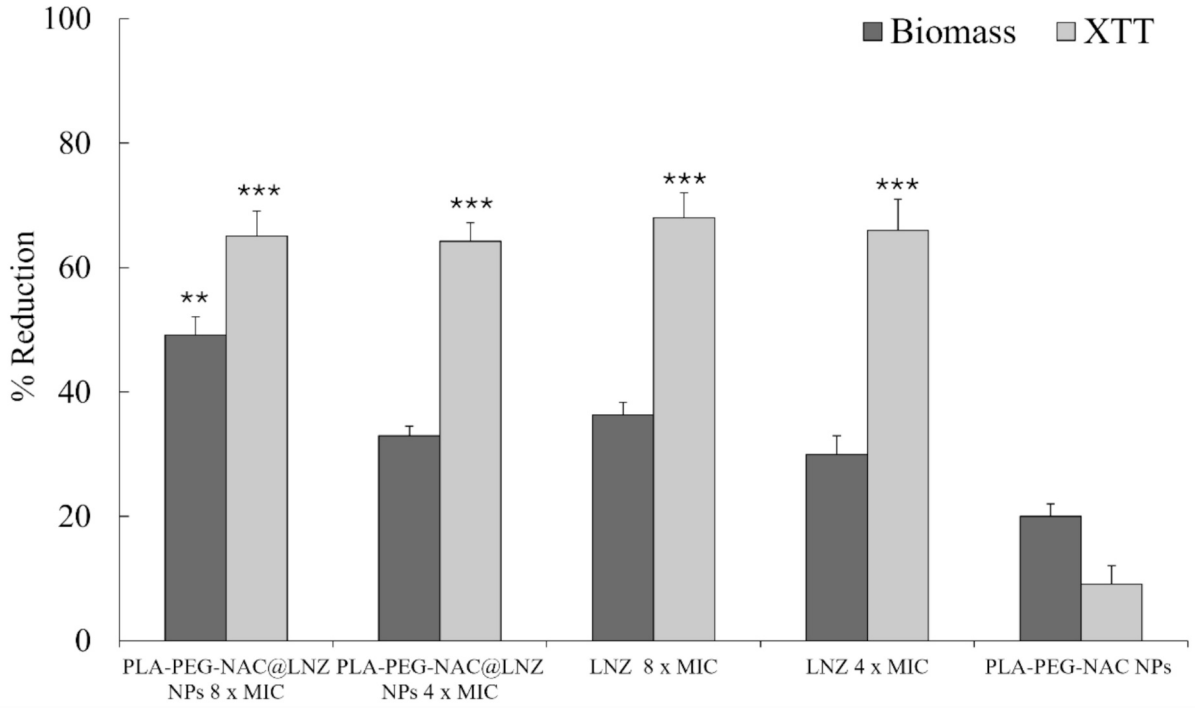

Fig. 7. Reduction of *S. aureus* MRSA ATCC 43300 early 8 h- preformed biofilm in the presence of PLA-PEG-NAC@LNZ NPs, free LNZ at 8 × MIC and 4 × MIC, and empty PLA-PEG-NAC NPs evaluated by colorimetric and metabolic viability assay (XTT). Values are expressed as mean ± standard deviation of biofilm inhibition (%). Pairwise comparisons with the control (Tukey's test) are indicated as follows: ** ($p < 0.01$); *** ($p < 0.001$).

activity of PLA-PEG-NAC@LNZ NPs was comparable to free LNZ, the drug release profile should be taken in account (Fig. 3) and specifically should be considered that in the first 24 h (which corresponds to the timeframe of our biological assays) about 78% of LNZ was released from NPs and it can be considered the pharmacologically active fraction during that period. Therefore, the activity of LNZ embedded in NPs was preserved.

3.5. Effect of PLA-PEG-NAC@LNZ NPs on biofilm formation

The effects of sub-MIC concentrations of PLA-PEG-NAC@LNZ NPs and free LNZ on biofilm formation are reported in Fig. 5.

At 0.5 × MIC, PLA-PEG-NAC@LNZ NPs showed significantly greater inhibition (62%) than free LNZ (39%) compared with the untreated control. Interestingly, this effect was partially maintained at 0.25 × MIC, where PLA-PEG-NAC@LNZ NPs achieved 45% inhibition, more than double that observed for free LNZ (21%). By contrast, unloaded PLA-PEG-NAC NPs exerted a negligible effect (<5%).

Fluorescence microscopy analysis confirmed the enhanced biofilm inhibition exerted by PLA-PEG-NAC@LNZ NPs compared to free LNZ at sub-MIC concentrations (Fig. 6 and Fig. S10). Specifically, *S. aureus* (MRSA) treated with PLA-PEG-NAC@LNZ NPs and free LNZ at both 0.5 × MIC and 0.25 × MIC formed biofilms with reduced cellular density and decreased viability (green fluorescence), compared to the dense,

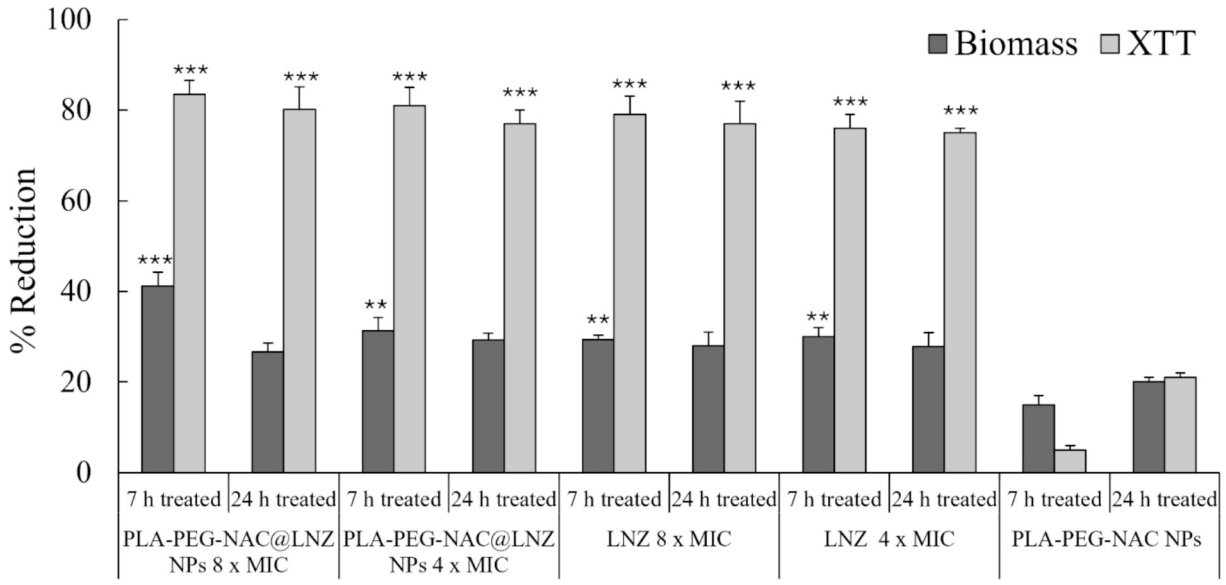

Fig. 8. Reduction of *S. aureus* MRSA ATCC 43300 late 24 h- preformed biofilm treated for 7 h or 24 h with 8 × MIC or 4 x MIC of PLA-PEG-NAC@LNZ NPs, free LNZ, and empty PLA-PEG-NAC NPs, evaluated by colorimetric and metabolic viability assay (XTT). Values are expressed as mean ± standard deviation of biofilm inhibition (%). Pairwise comparisons with the control (Tukey's test) are indicated as follows: ** ($p < 0.01$); *** ($p < 0.001$).

highly viable biofilms observed under control conditions (TSBG and empty NPs). Notably, this effect was more pronounced in biofilms treated with PLA-PEG-NAC@LNZ NPs than in those treated with free LNZ.

The mode of action of LNZ against planktonic cells is well understood; however, its mechanism of action against biofilms remains less clear. Previous studies assessing the anti-biofilm activity of LNZ have focused mainly on free LNZ, with only a few papers investigating its effectiveness when delivered through nanoformulations [29], due to the short development history of oxazolidinones, and their use as last resort antibiotics. Interestingly, our results showed that PLA-PEG-NAC NPs incorporating LNZ exhibited a superior ability to inhibit MRSA biofilm formation than free LNZ, likely due to improved drug solubility and permeability.

3.6. Effect of PLA-PEG-NAC@LNZ NPs on biofilm-embedded MRSA

PLA-PEG-NAC@LNZ NPs at 8 × MIC significantly reduced biofilm biomass (49%) compared with the untreated control (Fig. 7). At 4 × MIC, both PLA-PEG-NAC@LNZ NPs and free LNZ showed a comparable trend of biomass reduction (33% and 30%, respectively). Minimal activity was also observed for empty PLA-PEG-NAC NPs (without LNZ). Conversely, both PLA-PEG-NAC@LNZ NPs and free LNZ caused a significant reduction in metabolic activity (65–68%), whereas empty PLA-PEG-NAC NPs showed a negligible effect. The discrepancy between biomass and metabolic activity percentage reduction (XTT, Fig. 7) may be explained by the fact that biomass quantification methods account for both viable and non-viable bacteria within the biofilm. This interpretation was supported by the different effects observed for empty PLA-PEG-NAC NPs (without LNZ) on biomass and metabolic activity.

Fig. 8 reported the effects of two treatments (7 and 24 h) on mature MRSA biofilms exposed to PLA-PEG-NAC@LNZ NPs and free LNZ at 8 × and 4 × MIC. Notably, the most pronounced and statistically significant effect was observed with PLA-PEG-NAC@LNZ NPs at 8 × MIC after 7 h of treatment, resulting in 41% reduction in biofilm biomass. The remaining treatments caused comparable levels of biofilm reduction (25–30%), regardless of treatment duration. In all cases, a significant decrease in metabolic activity was observed, ranging from 75% to 85%.

We recently demonstrated that PLA-PEG NPs act as an enhancer of LNZ activity against 24 h- preformed biofilms [11]. The results of the present work confirmed these findings; nevertheless, given the relatively low NAC content (about 10 μg/mg), we did not observe a strong impact on the biological activity compared to non-functionalized PLA-PEG NPs. Rather, NAC functionalization was intended to modulate polymer properties without dramatically altering the biological profile. Therefore, while the chemical incorporation was well-established, the direct biological benefit of NAC as an added functional component has not been conclusively demonstrated since the moderate grafting did not produce a strong enhancement of biological activity compared to unmodified ("bare") PLA-PEG NPs, but rather it may modify polymer features and contribute subtly to the observed effects. Further improvements of the antibiofilm activity could be achieved by increasing NAC concentration in the polymeric NPs, either by modifying the synthetic pathway for NAC conjugation or through physical encapsulation. For covalent conjugation, one promising strategy would involve modifying the polymer end-groups with dendrimeric or branched moieties (e.g., trizma, bis-MPA, or citric acid) to increase NAC grafting density at the polymer end chain. Physical encapsulation of NAC within the nanoparticle core could be optimized by leveraging established formulation strategies reported in literature [30]. These approaches will be explored in future studies.

Table 2
Antibacterial activity of combination of free drugs and combination of PLA-PEG-NAC@LNZ NPs with PLA-PEG-NAC@Pent NPs by the checkerboard test and calculation of the fractional inhibitory concentration (FIC) index.

	E. coli ATCC 10536		
	MIC	BEST COMBINATION	FIC Index
	μg/mL		
LNZ	64	16	0.5
Pent	32	8	
PLA-PEG-NAC@LNZ NPs	64	8	0.625
PLA-PEG-NAC@Pent NPs	32	16	

3.7. Checkerboard test

Co-encapsulation of two drugs into polymeric nanoparticles is well known to be challenging, often resulting in very low drug loading [31]. Our experimental results confirmed this limitation for PLA-PEG-NAC

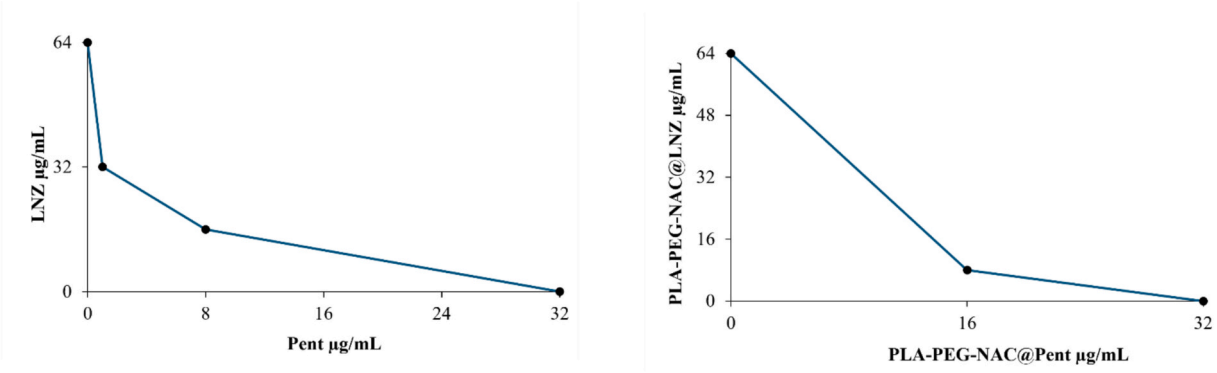

Fig. 9. Isobolograms depicting the effect of LNZ in combination with Pent against *E. coli* ATCC 10536, determined by the checkerboard test and calculation of the fractional inhibitory concentration (FIC). Left: combination of free LNZ and free Pent; right: combination of PLA-PEG-NAC@LNZ NPs and PLA-PEG-NAC@Pent NPs.

NPs (data not shown). Consequently, the PLA-PEG-NAC@LNZ@Pent formulation was not further pursued. As an alternative strategy, we studied the antimicrobial effect of a blended mixture of PLA-PEG-NAC@LNZ NPs and PLA-PEG-NAC@Pent NPs.

LNZ and Pent incorporated into the PLA-PEG-NAC NPs showed an activity against *E. coli* comparable to that of the free drugs. The combination of LNZ and Pent in their free form exhibited a synergistic effect (FIC index = 0.5), whereas the combination of PLA-PEG-NAC@LNZ NPs and PLA-PEG-NAC@Pent NPs demonstrated an additive effect (FIC index = 0.625) (Table 2 and Fig. 9).

These results confirmed the adjuvant activity of Pent in enhancing the susceptibility of *E. coli* to LNZ. Specifically, Pent and LNZ alone exhibited MICs of 32 µg/mL and 64 µg/mL, respectively. However, when assayed in combination, the MIC was reduced fourfold, demonstrating a synergistic effect. This finding aligned with previously reported studies [15,16]. Moreover, drug combinations offer further benefits, such as a slower emergence of bacterial resistance likely due to additional multitargeting mechanisms [32].

Although the combination of our PLA-PEG-NAC@Pent NPs and PLA-PEG-NAC@LNZ NPs demonstrated an additive effect, this result should be interpreted in the context of the release profile (Fig. 3). Notably, approximately 78% of LNZ was released from the NPs within the first 24 h (which corresponds to the timeframe of our biological assays), whereas Pent exhibited a slower release, with only 25% released from PLA-PEG-NAC@Pent NPs over the same period. Therefore, 78% of LNZ and 25% of Pent released within 24 h can be considered the pharmacologically active fraction.

The release kinetics of both agents are governed by the same carrier matrix, which results in comparable diffusion-controlled profile as suggested by kinetic parameters obtained from the fitting analysis. The significant difference in drug release percentages, likely related to distinct chemical and physicochemical properties of LNZ and Pent, may influence the observed additive effect against *E. coli* and the timing of their synergistic action, being the slower release of Pent a limiting factor. To investigate this aspect, we performed also a checkboard assay (data not reported) in which PLA-PEG-NAC@Pent NPs were added to the bacterial culture 30 min prior to PLA-PEG-NAC@LNZ NPs, aiming to exploit the membrane-permeabilizing effect of Pent. The very slow release of Pent from the nanoparticles suggested that its delayed availability may limit its potentiating role.

Based on these observations, we believe that future optimization of this nanoplatform might benefit from replacing Pent with alternative antibiotic potentiators or enhancers characterized by more favorable release kinetics. Recent studies have demonstrated that the combination of LNZ with adjuvants or potentiators, such as Arg–biodynamers [33], ε–poly-L-lysine [34], or polymyxin B [35,36], can broaden the antibacterial spectrum against Gram-negative bacteria by increasing membrane permeability or facilitating intracellular uptake, resulting in additive to synergistic effects depending on the system and the bacterial strain. Such approaches can enhance therapeutic outcomes by providing an early burst of the potentiator followed by a sustained release of the primary drug.

In conclusion, our study demonstrated the efficacy of PLA-PEG-NAC@LNZ NPs against MRSA biofilms, as well as the ability of the dual antibacterial drug-loaded nanoformulation to broaden the antibacterial spectrum of LNZ. Moreover, cytotoxicity assays in Vero cells demonstrated no notable toxicity of PLA-PEG-NAC NPs, either in their drug-loaded or unloaded forms, supporting their potential suitability for further studies.

In perspective, *in vivo* validation using infection models in mice will be essential to confirm the therapeutic potential (antibacterial efficacy, biodistribution, therapeutic outcomes) and safety of the proposed nanoantibiotics in a biologically relevant context.

CRediT authorship contribution statement

Antonia Nostro: Writing – review & editing, Writing – original draft, Data curation, Conceptualization. **Giovanna Ginestra:** Investigation. **Federica Grasso:** Investigation. **Massimiliano Cordaro:** Investigation. **Anna Piperno:** Writing – review & editing, Formal analysis. **Angelo Nicosia:** Writing – review & editing, Investigation. **Angela Scala:** Writing – review & editing, Writing – original draft, Visualization, Validation, Supervision, Data curation, Conceptualization.

Declaration of competing interest

The authors declare that they have no known competing financial interests or personal relationships that could have appeared to influence the work reported in this paper.

Acknowledgments

The authors sincerely thank Placido Giuseppe Mineo (University of Catania), Antonino Mazzaglia and Giuseppe Nocito (CNR-ISMN, URT of Messina), Lucia Cambria (University of Messina) for fruitful discussion and comments.

Appendix A. Supplementary material

Supplementary data to this article can be found online at https://doi.org/10.1016/j.eurpolymj.2026.114780.

Data availability

Data will be made available on request.

References

[1] K. Wang, K. Amin, Z. An, Z. Cai, H. Chen, Advanced functional polymer materials, Mater. Chem. Front. 4 (2020) 1803–1915, https://doi.org/10.1039/D0QM00025F.

[2] M.A. Gauthier, M.I. Gibson, H.-A. Klok, Synthesis of functional polymers by post-polymerization modification, Angew. Chem. Int. Ed. 48 (2009) 48–58, https://doi.org/10.1002/anie.200801951.

[3] M. Chrószcz-Porebska, A. Gadomska-Gajadhur, Cysteine conjugation: an approach to obtain polymers with enhanced muco- and tissue adhesion, Int. J. Mol. Sci. 25 (2024) 12177, https://doi.org/10.3390/ijms252212177.

[4] A. Manoharan, T. Das, G.S. Whiteley, T. Glasbey, F.H. Kriel, J. Manos, The effect of N-acetylcysteine in a combined antibiofilm treatment against antibiotic-resistant *Staphylococcus aureus*, J. Antimicrob. Chemother. 75 (2020) 1787–1798, https://doi.org/10.1093/jac/dkaa093.

[5] Y. Jun, C.K. Youn, E.R. Jo, S.I. Cho, In vitro inhibitory activity of N-acetylcysteine on tympanostomy tube biofilms from methicillin-resistant *Staphylococcus aureus* and quinolone-resistant *Pseudomonas aeruginosa*, Int. J. Pediatr. Otorhinolaryngol. 126 (2019) 109622, https://doi.org/10.1016/j.ijporl.2019.109622.

[6] F. Costa, D.M. Sousa, P. Parreira, et al., N-acetylcysteine-functionalized coating avoids bacterial adhesion and biofilm formation, Sci. Rep. 7 (2017) 17374, https://doi.org/10.1038/s41598-017-17310-4.

[7] B. Malaekeh-Nikouei, B.S.F. Bazzaz, E. Mirhadi, A.S. Tajani, B. Khameneh, The role of nanotechnology in combating biofilm-based antibiotic resistance, J. Drug Deliv. Sci. Technol. 60 (2020) 101880, https://doi.org/10.1016/j.jddst.2020.101880.

[8] Y. Liu, L. Shi, L. Su, H.C. van der Mei, P.C. Jutte, Y. Ren, H.J. Busscher, Nanotechnology-based antimicrobials and delivery systems for biofilm-infection control, Chem. Soc. Rev. 48 (2019) 428–446, https://doi.org/10.1039/c7cs00807d.

[9] G. Landini, T. Di Maggio, F. Sergio, et al., Effect of high N-acetylcysteine concentrations on antibiotic activity against a large collection of respiratory pathogens, Antimicrob. Agents Chemother. 60 (2016) 7513–7517, https://doi.org/10.1128/AAC.01334-16.

[10] A. Bernkop-Schnurch, Thiomers: a new generation of mucoadhesive polymers, Adv. Drug Delivery Rev. 57 (2005) 1569–1582, https://doi.org/10.1016/j.addr.2005.07.002.

[11] R. Oliva, G. Ginestra, A. Piperno, A. Mazzaglia, A. Nostro, A. Scala, Harnessing the power of PLA-PEG nanoparticles for Linezolid delivery against methicillin-resistant *Staphylococcus aureus*, Int. J. Pharmac. 642 (2023) 123067, https://doi.org/10.1016/j.ijpharm.2023.123067.

[12] C. Foti, A. Piperno, A. Scala, O. Giuffrè, Oxazolidinone antibiotics: chemical, biological and analytical aspects, Molecules 26 (2021) 4280, https://doi.org/10.3390/molecules26144280.

[13] A. Scala, A. Piperno, N. Micale, P.G. Mineo, A. Abbadessa, R. Risoluti, G. Castelli, F. Bruno, F. Vitale, A. Cascio, G. Grassi, "Click" on PLGA-PEG and hyaluronic acid: Gaining access to anti-leishmanial pentamidine bioconjugates, J. Biomed. Mater. Res. Part B 106 (2018) 2778–2785, https://doi.org/10.1002/jbm.b.34058.

[14] N. Micale, A. Piperno, N. Mahfoudh, U. Schurigt, M. Schultheis, P.G. Mineo, T. Schirmeister, A. Scala, G. Grassi, A hyaluronic acid–pentamidine bioconjugate as a macrophage mediated drug targeting delivery system for the treatment of leishmaniasis, RSC Adv. 5 (2015) 95545–95550, https://doi.org/10.1039/C5RA18019H.

[15] M. Tang, D. Zhao, S. Liu, X. Zhang, Z. Yao, H. Chen, C. Zhou, T. Zhou, C. Xu, The properties of linezolid, rifampicin, and vancomycin, as well as the mechanism of action of pentamidine, determine their synergy against gram-negative bacteria, Int. J. Mol. Sci. 24 (2023) 13812, https://doi.org/10.3390/ijms241813812.

[16] M. Tang, C. Qian, X. Zhang, Y. Liu, W. Pan, Z. Yao, W. Zeng, C. Xu, T. Zhou, When combined with pentamidine, originally ineffective linezolid becomes active in carbapenem-resistant enterobacteriaceae, Microbiol. Spectr. 11 (2023) 03138, https://doi.org/10.1128/spectrum.03138-22.

[17] Clinical and Laboratory Standards Institute (CLSI). Performance Standards for Antimicrobial Susceptibility Testing. 30th ed. CLSI Supplement M100. Wayne, PA: Clinical and Laboratory Standards Institute; 2020.

[18] A. Nostro, A.S. Roccaro, G. Bisignano, A. Marino, M.A. Cannatelli, F.C. Pizzimenti, P.L. Cioni, F. Procopio, A.R. Blanco, Effects of oregano, carvacrol and thymol on *Staphylococcus aureus* and *Staphylococcus epidermidis* Biofilms, J. Med. Microbiol. 56 (2007) 519–523, https://doi.org/10.1099/jmm.0.46804-0.

[19] E. Marini, M. Di Giulio, G. Ginestra, G. Magi, S. Di Lodovico, A. Marino, B. Facinelli, L. Cellini, A. Nostro, Efficacy of carvacrol against resistant rapidly growing mycobacteria in the planktonic and biofilm growth mode, PLoS One 14 (2019) e0219038, https://doi.org/10.1371/journal.pone.0219038.

[20] E. Marini, M. Di Giulio, G. Magi, S. Di Lodovico, M.E. Cimarelli, A. Brenciani, A. Nostro, L. Cellini, B. Facinelli, Curcumin, an antibiotic resistance breaker against a multiresistant clinical isolate of *mycobacterium abscessus*, Phytother. Res. 32 (2018) 488–495, https://doi.org/10.1002/ptr.5994.

[21] EUCAST. Terminology Relating to Methods for the Determination of Susceptibility of Bacteria to Antimicrobial Agents. Clin. Microbiol. Infect. 6 (2000) 503–508.

[22] A. Scala, A. Piperno, S.M. Torcasio, A. Nicosia, P.G. Mineo, G. Grassi, "Clickable" polylactic acids obtained by solvent free intra-chain amidation, Eur. Polymer J. 109 (2018) 341–346, https://doi.org/10.1016/j.eurpolymj.2018.10.004.

[23] A. Nicosia, G. La Perna, L.M. Cucci, C. Satriano, P.G. Mineo, A multifunctional conjugated polymer developed as an efficient system for differentiation of SH-SY5Y tumour cells, Polymers 14 (2022) 4329, https://doi.org/10.3390/polym14204329.

[24] F. Vento, A. Privitera, G. Caruso, A. Nicosia, A silibinin-poly(ε-caprolactone) conjugate as an enhanced anticancer agent, Macromol. Biosci. 25 (2025) 2400510, https://doi.org/10.1002/mabi.202400510.

[25] C. Bento, M. Katz, M.M.M. Santos, C.A.M. Afonso, Striving for uniformity: a review on advances and challenges to achieve uniform polyethylene glycol, Org. Process Res. Dev. 28 (2024) 860–890, https://doi.org/10.1021/acs.oprd.3c00428.

[26] S.M. Torcasio, R. Oliva, M. Montesi, S. Panseri, G. Bassi, A. Mazzaglia, A. Piperno, O. Coulembier, A. Scala, Three-armed RGD-decorated starPLA-PEG nanoshuttle for docetaxel delivery, Biomater. Adv. 140 (2022) 213043, https://doi.org/10.1016/j.bioadv.2022.213043.

[27] L.T.T. Nguyen, M.T. Gokmenac, F.E. Du Prez, Kinetic comparison of 13 homogeneous thiol–X reactions, Polym. Chem. 4 (2013) 5527–5536, https://doi.org/10.1039/C3PY00743J.

[28] P. Trucillo, Drug carriers: a review on the most used mathematical models for drug release, Processes 10 (2022) 1094, https://doi.org/10.3390/pr10061094.

[29] A.R.N. Ndukwe, S. Wiedbrauk, N.R.B. Boase, K.E. Fairfull-Smith, Strategies to improve the potency of oxazolidinones towards bacterial biofilms, Chem. Asian J. 17 (2022) e202200201, https://doi.org/10.1002/asia.202200201.

[30] R.M. Pinto, C. Monteiro, S.A. Costa Lima, S. Casal, P. Van Dijck, M.C.L. Martins, C. Nunes, S. Reis, N-acetyl-l-cysteine-loaded nanosystems as a promising therapeutic approach toward the eradication of *Pseudomonas aeruginosa* biofilms, ACS Appl. Mater. Interfaces 13 (2021) 42329–42343, https://doi.org/10.1021/acsami.1c05124.

[31] S. Bhattacharjee, Craft of co-encapsulation in nanomedicine: a struggle to achieve synergy through reciprocity, ACS Pharmacol. Transl. Sci. 5 (2022) 278–298, https://doi.org/10.1021/acsptsci.2c00033.

[32] Y. Zhou, W. Huang, E. Lei, A. Yang, Y. Li, K. Wen, M. Wang, L. Li, Z. Chen, C. Zhou, S. Bai, J. Han, W. Song, X. Ren, X. Zeng, H. Pu, M. Wan, X. Feng, Cooperative membrane damage as a mechanism for pentamidine-antibiotic mutual sensitization, ACS Chem. Biol. 17 (2022) 3178–3190, https://doi.org/10.1021/acschembio.2c00613.

[33] M.A.M. Kamal, J. Bassil, et al., Arg-biodynamers as antibiotic potentiators through interacting with Gram-negative outer membrane lipopolysaccharides, Eur. J. Pharm. Biopharm. 200 (2024) 114336.

[34] G.G. Kaya, S. Medaglia, V. Candela-Noguera, M.Á. Tormo-Mas, M.D. Marcos, E. Aznar, H. Deveci, R. Martínez-Máñez, Antibacterial activity of linezolid against gram-negative bacteria: utilization of ε-poly-l-lysine capped silica xerogel as an activating carrier, Pharmaceutics 12 (2020) 1126, https://doi.org/10.3390/pharmaceutics12111126.

[35] T. Huang, M. Zeng, H. Fu, K. Zhao, T. Song, Y. Guo, J. Zhou, L. Zhai, C. Liu, B. Prithiviraj, X. Wang, Y. Chu, A novel antibiotic combination of linezolid and polymyxin B octapeptide PBOP against clinical *Pseudomonas aeruginosa* strains, Ann. Clin. Microbiol. Antimicrob. 21 (2022) 38, https://doi.org/10.1186/s12941-022-00531-5.

[36] I. Otri, S. Medaglia, R. Martínez-Máñez, E. Aznar, F. Sancenón, Exploring the synergy between nano-formulated linezolid and polymyxin B as a gram-negative effective antibiotic delivery system based on mesoporous silica nanoparticles, Nanomaterials 14 (2024) 228, https://doi.org/10.3390/nano14020228.